NPG Asia Materials (2012) 4, e2; doi:10.1038/am.2012.2

www.nature.com/am

ORIGINAL ARTICLE

Wurtzite $Cu_2ZnSnSe_4$ nanocrystals for high-performance organic–inorganic hybrid photodetectors

Jian-Jun Wang, Jin-Song Hu, Yu-Guo Guo and Li-Jun Wan

Indium-free quaternary chalcogenide, $Cu_2ZnSnSe_4$ (CZTSe), has driven much attention for its potential application in photovoltaics and optoelectronics. It is well known that the composition and structure of nanocrystals (NCs) significantly affect their optical and electrical properties. Controllable synthesis of materials with new crystal structures, especially metastable structures, has given impetus to the development of nanomaterials with many new exciting properties and applications. High-quality CZTSe NCs with thermodynamically metastable wurtzite phase and optical band gap of 1.46 eV were herein synthesized via a facile, lost-cost and safe-solution method. The formation mechanism of the wurtzite CZTSe NCs was investigated in detail, which indicates high reaction rate and low surface energy are favorable for the formation of wurtzite structure. The promising application of as-synthesized NCs in photovoltaics and optoelectronics has been demonstrated by the high-performance hybrid photodetector made from CZTSe NCs and P3HT, with an on/off ratio larger than 150.
NPG Asia Materials (2012) **4,** e2; doi:10.1038/am.2012.2; published online 18 January 2012

Keywords: chalcogenide; nanocrystal; photodetector; photovoltaic; wurtzite

INTRODUCTION

Colloidal nanocrystals (NCs) have been considerably investigated and demonstrated the promising applications in solar energy conversion, optoelectronic devices and ultrasensitive detection due to their low cost and easily scalable production, as well as unique chemical and physical properties.[1–4] On the other hand, colloidal NCs can be well dispersed in many solvent and deposited to films via low cost process such as spin-casting, dip-coating and printing, and easily mixed with polymers to form hybrid light-absorbing layers with enhanced performance.[5–9] An important parameter in their use is the band gap energy of NCs, which can be tuned by their size, shape and composition.[10,11] Many attractive colloidal NCs, including SnSe, PbS and I-III-VI_2 NCs and so on, have been prepared in consideration of band gap optimization for wider solar spectral response.[5,8,12–16] Among them, I-III-VI_2, especially copper indium diselenide ($CuInSe_2$), is proven a very promising light-absorbing materials in photoelectric devices, because of their high optical-absorption coefficients and versatile optical and electrical characteristics, which can in principle, be manipulated and tuned for a specific need in a given device.[17] The nearly 20% energy conversion efficiency of $CuInSe_2$-based single-junction solar cells has been demonstrated.[18] However, the supply of the rare metal indium will be a trouble for terawatt energy demand in the near future.

Recently, indium-free quaternary chalcogenides (Cu_2ZnSnS_4, $Cu_2ZnSnSe_4$ (CZTSe)) have driven much attention for their potential application in low-cost solar cells due to their many advantages including an appropriate direct band gap (1.0–1.5 eV), high absorption coefficient (up to $10^5\,cm^{-1}$), extremely low toxicity, high radiation stability, as well as relative abundance (indium-free) of its elements. In addition, CZTSe films have promising thermoelectric properties, with large thermoelectric figure of merit values of about 0.9 at 860 K.[19] Several solution-based methods have been reported to synthesize nearly stoichiometric Cu_2ZnSnS_4 NCs.[20–22] The conversion efficiency of the Cu_2ZnSnS_4-absorber films prepared by co-sputtering, which added cost to the process, has reached over 6.7%.[23] Moreover, $Cu_2ZnSnS_xSe_{4-x}$-based thin-film solar cells with power conversion efficiency of 9.6%, a level suitable for possible commercialization, have been constructed by solution method using toxic and unstable hydrazine.[24] However, solution-based methods for synthesis of high-quality and stoichiometric CZTSe NCs is still a big challenge.[25,26] On the other hand, it is well known that the composition and structure of NCs significantly affect their optical and electrical properties, and the structure can be tuned by source materials, capping ligands, as well as synthetic temperature.[8,13,14,27,28] The reported $Cu_2ZnSn(S,Se)_4$ NCs mostly show the stannite or kesterite structures.[19–22,25] Recently, Li and coworkers[26] reported the Cu_2ZnSnS_4 NCs with wurtzite

Key Laboratory of Molecular Nanostructure and Nanotechnology and Beijing National Laboratory for Molecular Sciences (BNLMS), Institute of Chemistry, Chinese Academy of Sciences (CAS), Beijing, PR China
Correspondence: Professor Y-G Guo or Professor L-J Wan, Institute of Chemistry, Chinese Academy of Sciences (CAS), Number 2, North 1st Street, Zhongguancun, Beijing 100190, PR China.
E-mail: ygguo@iccas.ac.cn or wanlijun@iccas.ac.cn
Received 19 August 2011; revised 26 October 2011; accepted 31 October 2011

structure, which has been found in many binary and ternary chalcogenides, but seldom in quaternary compounds.[8,13,14,29,30] The wurtzite structure owns disordered cations, and the random distribution of A and B ions in the wurtzite phase offers the flexibility for stoichiometry control, which is advantageous for the fabrication of photovoltaic devices, as it provides the ability to tune energy band gap for device optimization.[30] Therefore, controllable synthesis of materials with new crystal structures, especially metastable structures such as wurtzite, is opening up an avenue to develop nanomaterials with new exciting properties and applications.[8,11,14,27,30] This encourages us to investigate the formation of ternary and multiple component chalcogenides with wurtzite structure. In this paper, we, for the first time, reported the synthesis of CZTSe quaternary NCs with wurtzite structure, their formation mechanism and the use in high-performance hybrid photodetector.

MATERIALS AND METHODS

Materials

$CuCl_2{\cdot}2H_2O$, $InCl_3{\cdot}5H_2O$, sodium oleate, $ZnCl_2$, hexane, toluene and P3HT (Mn, 20000, Mw, 33000) were analytical reagent grade, bought from the Beijing Chemical Factory, Beijing, China. Tin (II) 2-ethylhexanoate (96%) and diphenyl diselenide (98%) were purchased from Alfa-Aesar, Tianjing, China. Oleylamine was technical grade from Fluka, Shanghai, China. All chemicals were used directly without any purification.

Methods

In a typical synthesis, diphenyl diselenide was selected as a selenide source. Stoichiometric amounts of diphenyl diselenide (0.25 mmol), Cu-oleate (0.25 mmol), Zn-oleate, Tin (II) 2-ethylhexanoate and 8-ml oleylamine were added into a 25-ml three-neck flask in air, and degassed by bubbling with Ar gas while stirring at ~70 and ~140 °C, respectively, for 30 min. The precursor mixture was heated to react at 255 °C for 40 min and then cooled down to room temperature. A volume of 5 ml of ethanol was added into the reaction mixture and the NCs were collected by centrifuging at 8000 r.p.m. for 3 min. After washing by another two volume of 5 ml of ethanol and centrifuging, the precipitate was redispersed in 5-ml toluene to form an ink solution for characterizations.

Characterization

The size and morphology of the NCs and high-resolution transmission electron microscopy (TEM) images were characterized by using Tecnai G2 20S-TWIN and Tecnai G2 F20 X-Twin microscope (FEI Company, Hillsboro, OR, USA), working at an accelerating voltage of 200 kV. The phase and the crystallographic structure of the NCs were characterized by powder X-ray diffraction (XRD), using a Regaku D/Max-2500 diffractometer equipped with a Cu Kα1 radiation (λ=1.54056 Å, Rigaku Corporation, Tokyo, Japan). The simulated CZTSe powder XRD patterns were obtained by using General Structure Analysis System (GSAS, A.C. Larson and R.B. Von Dreele, Los Alamos National Laboratory). The composition of the as-synthesized NCs was analyzed by energy dispersive X-ray spectrometry, using a GENESIS system (EDAX Inc., Mahwah, NJ, USA) attached to the TEM. UV-vis absorption spectra were recorded at room temperature with a Lambda 950 UV-vis spectrometer (Perkinelmer Ltd company, Wokingham, UK). X-ray photoelectron spectroscopy data were obtained with an ESCALab220i-XL electron spectrometer from VG Scientific (East Grinstead, UK) using a 300 W AlKα radiation. The morphology of the films was characterized by scanning electron microscopy (SEM JOEL 6701, JEOL Ltd, Tokyo, Japan). Current-voltage (I–V) characteristics of the devices were recorded with a Keithley 4200 SCS (Keithley, Cleveland, OH, USA) and a Micromanipulator 6150 probe station (Carson City, NV, USA) in a shielded and clean box at room temperature. An iodine–tungsten lamp was selected as a white-light source in view of the significant absorption of the hybrid film in the wavelength range.

RESULTS AND DISCUSSION

The structure of the as-synthesized NCs was characterized by XRD, as shown in Figure 1a (pattern 1). It has been found that the XRD pattern cannot be indexed to any existing patterns in the standard JCPDS database. Preliminary simulation reveals that such NCs hold a wurtzite phase, which is totally different from the well-characterized stannite and kesterite phase in both JCPDS database and previous reports.[20–22,25] The experimental pattern of the CZTSe NCs matches well with the simulated one of wurtzite structure with a=4.00 Å and c=6.61 Å, which are smaller than those of $CuInSe_2$.[8]

To investigate the formation mechanism of the wurtzite CZTSe NCs, some control experiments were carried out. When the solvent was diluted by hexadecane, a non-coordinating solvent, during synthesis under otherwise identical conditions, the diffraction peak positions of the product matched the wurtzite CZTSe, although with some changes. The intensities of (002), (110) and (112) peaks, which are difficult to distinguish from the corresponding (112), (204) and (312) peaks of stannite-structure CZTSe NCs, became higher than expected, and the intensities of (102), (202) and (203) peaks, typical peaks of the wurtzite CZTSe NCs, became lower with the increase in amount of hexadecane. At the same time, the (008) peak indexed to

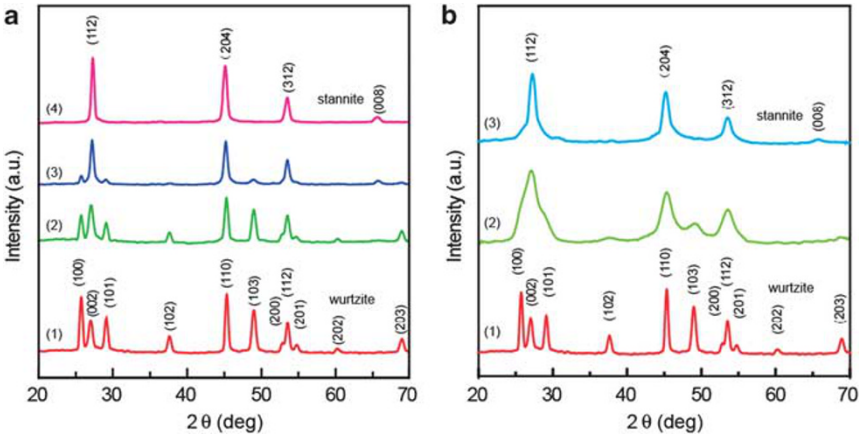

Figure 1 (**a**) X-ray diffraction (XRD) patterns of synthesized $Cu_2ZnSnSe_4$ nanocrystals (CZTSe NCs) in different solvents. (1) Oleylamine. (2) Oleylamine (6 ml) and hexadecane (2 ml). (3) Oleylamine (2 ml) and hexadecane (6 ml). (4) Oleic acid (2 ml) and hexadecane (6 ml). (**b**) XRD patterns of synthesized CZTSe NCs by using different Se sources at a heating rate of 10 °C min^{-1}. (1) Diphenyl diselenide. (2) Selenourea. (3) Se powder.

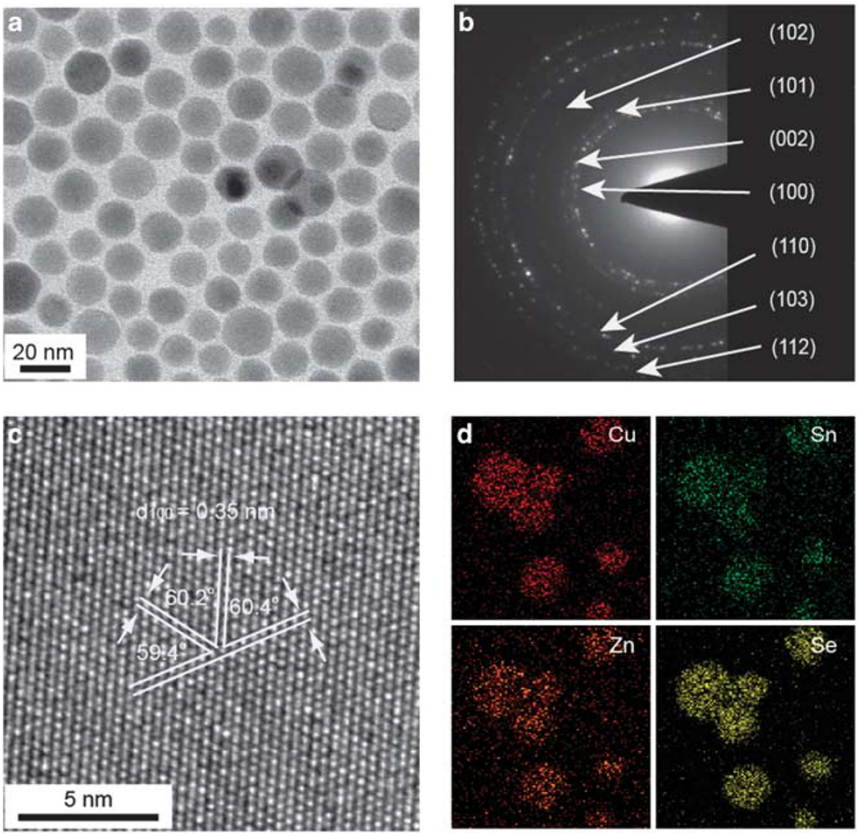

Figure 2 (**a**) Transmission electron microscopy (TEM) image of as-synthesized $Cu_2ZnSnSe_4$ nanocrystals (CZTSe NCs). (**b**) Selected area electron diffraction (SAED) pattern of as-synthesized CZTSe NCs. (**c**) High-resolution (HR) TEM image of a single CZTSe NC. (**d**) STEM-energy dispersive X-ray spectroscopy (EDS) elemental maps of CZTSe NCs.

stannite structure appeared (pattern 2 and 3, Figure 1a). Note that the existence of kesterite phase might not be excluded due to their similar XRD patterns. The above changes in the diffraction patterns implied that the resulted phases of the synthesized NCs underwent a conversion from wurtzite to stannite structure.[28] Similarly, Korgel and colleagues[31] has revealed polytypism in the nanodisks, with the wurtzite phase interfaced with significant chalcopyrite domains in $CuInS_2$ NCs. On the other hand, when the oleylamine in the mixed solvent was replaced by oleic acid, the synthesized CZTSe NC exhibited pure stannite as shown in Figure 1a (pattern 4). It has been predicted that Sn-containing quaternary chalcogenide compounds crystallize preferably in a sphalerite superstructure (zinc-blende-derived structures).[32] Hexagonal wurtzite CZTSe is a thermodynamically metastable phase, which is usually stable at very high temperature, whereas tetragonal stannite CZTSe is a more thermodynamically stable phase, which is stable at low temperature. Oleylamine is a strong ligand for Cu, Zn, Sn and Cd.[8,12,13,29,33] Therefore, oleylamine could promote the decomposition of metal compounds and cap the generated wurtzite crystal seeds to reduce the surface energy. These two factors contribute to the formation of the dynamically stable wurtzite phase. In addition, it is noted that the morphology of the synthesized NCs transformed from nanoparticle to nanowire, when oleylamine was substituted by oleic acid (Supplementary Figure S1). The transformation of the morphology consistently suggests the oleylamine molecule is a stronger stabilizer than oleic acid for the CZTSe NCs. Besides ligand molecule, it was found that Se source also significantly affected the final phase of the synthesized NCs. When diphenyl diselenide was substituted by selenourea or Se powder, while keeping all other experimental conditions same, the crystal structure of the as-synthesized NCs transformed from wurtzite to stannite (Figure 1b). It would be interesting to understand the effects of Se sources on the structure of product. By comparing three different Se sources, we think the influence of Se sources on the crystal structures of final product could be ascribed to the difference in reaction rates of Se sources, although the exact mechanism is still not very clear yet and need further investigation. It is obvious that diphenyl diselenide is most active among three Se sources, which leads to the highest reaction rate and is favored for generation of dynamically stable products at relatively low temperature. In contrast, Se powder is less active, due to no phenyl group, as an electron donor during the reaction with metal ions, resulting in lower reaction rate and the formation of thermodynamically stable stannite phase when Se powder was used as the Se source. When the reaction mixture was heated up at a low rate, the XRD pattern of the NCs synthesized by using diphenyl diselenide implies the slight distortion in wurtzite structure occurred in terms of the slight increase in intensity of (002) peak (corresponding to (112) peak in stannite structure), with no change of the morphology of NCs (Supplementary Figure S2). The phenomenon is in good agreement with the above facts. Furthermore, to prove the above conclusion, we synthesized a series of $CuInSe_2$ samples with solvent and Se powder controls, same as those for CZTSe. The XRD results confirmed the same influence of ligand molecule and activity of Se source on the phase of synthesized NCs (Supplementary Figure S3). From the above

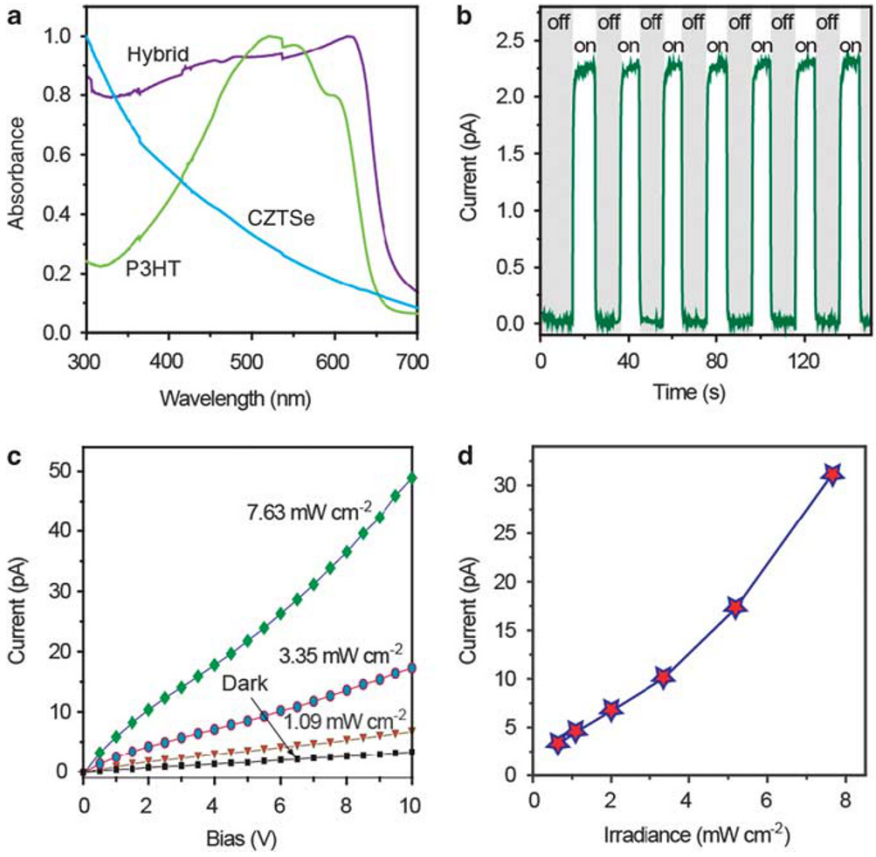

Figure 3 (**a**) UV-vis spectra of the P3HT film (green), $Cu_2ZnSnSe_4$ nanocrystal (CZTSe NC) film (blue) and P3HT:CZTSe hybrid film (weight ratio of 5:4, orange). (**b**) On/off switching of the hybrid device at an incident light density of 7.63 mW cm^{-2} and a bias voltage of 0.4 V. (**c**) Dark current and photocurrents at different incident light densities. (**d**) Measured photocurrents versus incident light densities at a bias voltage of 10 V.

control experiments, it can be concluded that the strong ligands promote the decomposition of metal compounds and are favored for reducing surface energy, and high activity of the Se source provides high reaction rate, which together make the dynamically stable products dominant. High reaction rate and low surface energy are indispensable for CZTSe NCs with a thermodynamically metastable wurtzite structure.

The preparation of monodispersed NCs is one of the pursuits in NC synthesis from both the chemistry perspectives and the application consideration. A modified synthesis procedure was developed to improve the monodispersity of as-synthesized CZTSe NCs in further experiments. The diphenyl diselenide was directly injected into the mixture of metal compounds at 190 °C, instead of adding into the initial reaction mixture to shorten the process of nucleation, followed by the same procedure as described in the Methods. Figure 2a and Supplementary Figure S4a show typical TEM images of the as-synthesized CZTSe NCs, which indicates that the NCs have much improved size distribution, with an average diameter of 19.3 ± 2.3 nm, compared with polydispersed NCs in previous synthesis. The selected area electron diffraction pattern (Figure 2b) is well consistent with the simulated wurtzite structure of CZTSe, and the XRD result also confirmed the NCs are wurtzite structure (Supplementary Figure S4b). Figure 2c presents an high-resolution TEM image of an individual NC. The lattice fringes show that the NC is a single crystal with a d-spacing of 0.35 nm indexed to the (100) plane of wurtzite CZTSe.

To identify the element distribution of the as-synthesized CZTSe NCs, scanning transmission electron microscopy-energy dispersive X-ray spectroscopy elemental maps were recorded from CZTSe NCs. The results shown in Figure 2d reveal that the four elements of Cu, Zn, Sn and Se exist in all NCs and exhibit no apparent element separation or aggregation, indicating that the distributions of all the four elements are very homogeneous within the NCs. X-ray photoelectron spectroscopy analysis shows that all the four elements are in the oxidation states as expected in CZTSe (Supplementary Figure S5). Additionally, the Cu/Zn/Sn/Se ratio measured with energy dispersive X-ray spectroscopy or X-ray photoelectron spectroscopyanalysis is close to the stoichiometry of CZTSe of 2:1:1:4 (Supplementary Figures S5 and S6). UV-vis absorption spectroscopy was recorded and used to estimate the band gap energy of the CZTSe NCs via the relation of $(\alpha h\nu)^2$ versus $h\nu$ (where α=absorbance, h=Planck constant and ν=frequency; Supplementary Figure S7). The result shows the effective band gap of the synthesized CZTSe NCs is 1.46 eV, which is consistent with those of the reported NCs synthesized by solution methods.[25,34]

Recently, hybrid organic–inorganic devices have attracted increasing attention for a logic choice to combine the unique properties of NCs with the easy film-forming property of organic polymers.[1,5–8,16,35,36] To test the potential application for photoelectric devices, the as-synthesized NCs were uniformly dispersed in P3HT matrix to form a three dimensional interconnected network, which leads to a large interface area favorable for charge carrier generation. The scanning electron microscopy images show that the hybrid film is highly

homogeneous (Supplementary Figure S8). From UV-vis spectra of the P3HT film (green), CZTSe NC film (blue) and P3HT:CZTSe NC hybrid film (weight ratio of 5:4; orange) as shown in Figure 3a, it can be seen that the inlay of CZTSe NCs into the P3HT film have significantly broaden the absorption spectra. Moreover, the absorption of hybrid film exhibits obvious red-shift derived from the reciprocity of the two components.[37–39]

The hybrid photodetector device was fabricated and measured as previously reported,[8,40] which exhibits excellent photoresponse characteristics as shown in Figure 3b. When the light irradiation was turned on and off, the current output of the device exhibits two distinct states, a 'low' current in the dark and a 'high' current under illumination. The switching between these two states was very fast and reversible, demonstrating the high performance as a highly sensitive photoswitch. In the dark, the NCs/P3HT film was nearly insulating with a dark current of 0.012 pA at 0.4 V, which implies an excellent cut-off capability. However, the current approaches 2.237 pA at an incident light density of 7.63 mW cm^{-2} and a bias voltage of 0.4 V. The on/off switching ratio is larger than 150. It should be noted that the 'on' current level is relative low, possibly due to long ligand covering the CZTSe NCs. The further investigation is still underway. For example, the short ligands such as pyridine or butylamine will be used to replace the long ligand, so as to facilitate the charge transfer/transport between organic polymer (P3HT) and inorganic NCs (CZTSe NCs). Moreover, photocurrent measurement of the device at different incident light densities further confirmed the high photosensitivity of the hybrid device. When the intensities of incident light were changed, the photocurrents of the device remarkably changed accordingly (Figure 3c). In this case, light is absorbed through the whole thickness of devices, and both the charge carriers are running within hybrid device, which agree well with previous reports on CdSe and $CuInSe_2$.[6,8] In addition, the analysis show that the current output of the photodetector exhibits strong dependence on light intensity, as shown in Figure 3d, which is similar to the reports on InSe and $CuInSe_2$.[8,16,40] The power dependence was calculated $\sim$1.20, that is, $I \sim P^{1.20}$, indicating superior photo-to-current capability of the hybrid material. The strong dependence on light intensity may be because the shorter wavelength light in white light source is high enough not only to eject an electron from a filled band of P3HT, but also to impart electron-sufficient kinetic energy for impact ionization. These results demonstrate the promising potential of the hybrid device as a photoswitch or a photodetector. It is worth noting that the applied bias voltage was of great importance for the on/off ratio of the device, which was related to the applied bias voltage dependence of the exciton dissociation and the background current of the device.[8]

In summary, a new facile and safe solution method was developed to synthesize high-quality wurtzite CZTSe NCs with lattice parameters of a=4.00 Å and c=6.61 Å, and an optical band gap of 1.46 eV. XRD, TEM, energy dispersive X-ray spectroscopy and X-ray photoelectron spectroscopy measurements confirmed the NCs were highly pure wurtzite CZTSe. The influence factors on the formation of wurtzite CZTSe NCs were investigated, which indicates high reaction rate and low surface energy are indispensable for the formation of CZTSe NCs with a thermodynamically metastable wurtzite phase. High-performance hybrid photodetectors were fabricated on the basis of the P3HT:CZTSe hybrid film. The device shows distinct 'ON' and 'OFF' state, with a ratio larger than 150 in photocurrents responding to the outside illumination. The high quality and optimum band gap of synthesized NCs make them promising candidates for hybrid devices, aiming at the applications in light detection and signal magnification for the development of low-cost, large area and flexible products.

ACKNOWLEDGEMENTS

This work was supported by the National Key Project on Basic Research (Grants 2011CB935700, 2009CB930400 and 2011CB808700), the National Natural Science Foundation of China (Grants 91127044, 20821003 and 21173237) and the Chinese Academy of Sciences.

1 Talapin, D. V, Lee, J. S., Kovalenko, M. V. & Shevchenko, E. V. Prospects of colloidal nanocrystals for electronic and optoelectronic applications. *Chem. Rev.* **110,** 389–458 (2009).
2 Kim, S- H., Lee, S. Y., Yang, S. M. & Yi, G. R Self-assembled colloidal structures for photonics. *NPG Asia Mater.* **3,** 25–33 (2011).
3 Li, J. F., Liu, W. S., Zhao, L. D. & Zhou, M. High-performance nanostructured thermoelectric materials. *NPG Asia Mater.* **2,** 152–158 (2010).
4 Chattopadhyay, S., Chen, L. C. & Chen, K. H. Energy production and conversion applications of one-dimensional semiconductor nanostructures. *NPG Asia Mater.* **3,** 74–81 (2011).
5 Franzman, M. A., Schlenker, C. W., Thompson, M. E & Brutchey, R. L Solution-phase synthesis of SnSe nanocrystals for use in solar cells. *J. Am. Chem. Soc.* **132,** 4060–4061 (2010).
6 Greenham, N. C., Peng, X. & Alivisatos, A. P. Charge separation and transport in conjugated-polymer/semiconductor-nanocrystal composites studied by photoluminescence quenching and photoconductivity. *Phys. Rev. B* **54,** 17628–17637 (1996).
7 Huynh, W. U., Dittmer, J. J. & Alivisatos, A. P. Hybrid nanorod-polymer solar cells. *Science* **295,** 2425–2427 (2002).
8 Wang, J. J., Wang, Y. Q., Cao, F. F., Guo, Y. G. & Wan, L. J. Synthesis of monodispersed wurtzite structure $CuInSe_2$ nanocrystals and their application in high-performance organic-norganic hybrid photodetectors. *J. Am. Chem. Soc.* **132,** 12218–12221 (2010).
9 Lee, B. Y., Sung, M. G., Lee, H., Namgung , S., Park, S. Y., Choi, D. S. & Hong, S. Integrated devices based on networks of nanotubes and nanowires. *NPG Asia Mater.* **2,** 103–111 (2010).
10 Regulacio, M. D. & Han, M. Y. Composition-tunable alloyed semiconductor nanocrystals. *Acc. Chem. Res.* **43,** 621–630 (2010).
11 Smith, A. M. & Nie, S. Semiconductor nanocrystals: structure, properties, and band gap engineering. *Acc. Chem. Res.* **43,** 190–200 (2010).
12 Baumgardner, W. J., Choi, J. J., Lim, Y. F. & Hanrath, T. SnSe nanocrystals: synthesis, structure, optical properties, and surface chemistry. *J. Am. Chem. Soc.* **132,** 9519–9521 (2010).
13 Norako, M. E. & Brutchey, R. L. Synthesis of metastable wurtzite CuInSe2 nanocrystals. *Chem. Mater.* **22,** 1613–1615 (2010).
14 Pan, D., An, L., Sun, Z., Hou, W., Yang, Y., Yang, Z. & Lu, Y. Synthesis of Cu-In-S ternary nanocrystals with tunable structure and composition. *J. Am. Chem. Soc.* **130,** 5620–5621 (2008).
15 Sargent, E. H. Infrared photovoltaics made by solution processing. *Nat. Photonics* **3,** 325–331 (2009).
16 Xue, D. J., Wang, J. J., Wang, Y. Q., Xin, S., Guo, Y. G. & Wan, L. J. Facile Synthesis of germanium nanocrystals and their application in organic–inorganic hybrid photodetectors. *Adv. Mater.* **23,** 3704–3707 (2011).
17 Tian, B., Kempa, T. J. & Lieber, C. M. Single nanowire photovoltaics. *Chem. Soc. Rev.* **38,** 16–24 (2008).
18 Saga, T. Advances in crystalline silicon solar cell technology for industrial mass production. *NPG Asia Mater.* **2,** 96–102 (2010).
19 Liu, M. L., Huang, F. Q., Chen, L. D. & Chen, I. W. A wide-band-gap p-type thermoelectric material based on quaternary chalcogenides of CuZnSnQ (Q=S, Se). *Appl. Phys. Lett.* **94,** 202103 (2009).
20 Guo, Q., Hillhouse, H. W. & Agrawal, R. Synthesis of Cu_2ZnSnS_4 nanocrystal ink and its use for solar cells. *J. Am. Chem. Soc.* **131,** 11672–11673 (2009).
21 Riha, S. C., Parkinson, B. A. & Prieto, A. L. Solution-based synthesis and characterization of Cu_2ZnSnS_4 nanocrystals. *J. Am. Chem. Soc.* **131,** 12054–12055 (2009).
22 Steinhagen, C., Panthani, M. G., Akhavan, V., Goodfellow, B., Koo, B. & Korgel, B. A. Synthesis of Cu_2ZnSnS_4 nanocrystals for use in low-cost photovoltaics. *J. Am. Chem. Soc.* **131,** 12554–12555 (2009).
23 Katagiri, H., Jimbo, K., Maw, W. S., Oishi, K., Yamazaki, M., Araki, H. & Takeuchi, A. Development of CZTS-based thin film solar cells. *Thin Solid Films* **517,** 2455–2460 (2009).
24 Todorov, T. K., Reuter, K. B. & Mitzi, D. B. High-efficiency solar cell with earth-abundant liquid-processed absorber. *Adv. Mater.* **22,** E156–E159 (2010).
25 Shavel, A., Arbiol, J. & Cabot, A. Synthesis of quaternary chalcogenide nanocrystals: stannite $Cu_2Zn_xSn_ySe_{1+x+2y}$. *J. Am. Chem. Soc.* **132,** 4514–4515 (2010).
26 Lu, X., Zhuang, Z., Peng, Q. & Li, Y. Wurtzite Cu_2ZnSnS_4 nanocrystals: a novel quaternary semiconductor. *Chem. Commun.* **47,** 3141–3143 (2011).
27 Deka, S., Genovese, A., Zhang, Y., Miszta, K., Bertoni, G., Krahne, R., Giannini, C. & Manna, L. Phosphine-free synthesis of p-type copper(I) selenide nanocrystals in hot coordinating solvents. *J. Am. Chem. Soc.* **132,** 8912–8914 (2010).
28 Batabyal, S. K., Tian, L., Venkatram, N., Ji, W. & Vittal, J. J. Phase-selective synthesis of $CuInS_2$ nanocrystals. *J. Phys. Chem. C.* **113,** 15037–15042 (2009).
29 Mahler, B., Lequeux, N. & Dubertret, B. Ligand-controlled polytypism of thick-shell CdSe/CdS nanocrystals. *J. Am. Chem. Soc.* **132,** 953–959 (2009).

30 Wang, Y. H., Zhang, X., Bao, N., Lin, B. & Gupta, A. Synthesis of shape-controlled monodisperse wurtzite $CuIn_xGa_{1-x}S_2$ semiconductor nanocrystals with tunable band gap. *J. Am. Chem. Soc.* **133,** 11072–11075 (2011).
31 Koo, B., Patel, R. N. & Korgel, B. A. Wurtzite- chalcopyrite polytypism in $CuInS_2$ nanodisks. *Chem. Mater.* **21,** 1962–1966 (2009).
32 Chen, S., Walsh, A., Luo, Y., Yang, J. H., Gong, X. G. & Wei, S. H. Wurtzite-derived polytypes of kesterite and stannite quaternary chalcogenide semiconductors. *Phys. Rev. B* **82,** 195203 (2010).
33 Yu, S. H. & Yoshimura, M. Shape and phase control of ZnS nanocrystals: template fabrication of wurtzite ZnS single-crystal nanosheets and ZnO flake-like dendrites from a lamellar molecular precursor $ZnS{\cdot}(NH_2CH_2CH_2NH_2)_{0.5}$. *Adv. Mater.* **14,** 296–300 (2002).
34 Riha, S. C., Parkinson, B. A. & Prieto, A. L. Compositionally tunable $Cu_2ZnSn(S_{1-x}Se_x)_4$ nanocrystals: probing the effect of Se-inclusion in mixed chalcogenide thin films. *J. Am. Chem. Soc.* **133,** 15272–15275 (2011).
35 Ramanathan, T., Abdala, A. A., Stankovich, S., Dikin, D. A., Herrera-Alonso, M., Piner, R. D., Adamson, D. H., Schniepp, H. C., Chen, X. & Ruoff, R. S. Functionalized graphene sheets for polymer nanocomposites. *Nat. Nanotechnol.* **3,** 327–331 (2008).
36 Sun, B., Marx, E. & Greenham, N. C. Photovoltaic devices using blends of branched CdSe nanoparticles and conjugated polymers. *Nano Lett.* **3,** 961–963 (2003).
37 Geng, J., Kong, B. S., Yang, S. B., Youn, S. C., Park, S., Joo, T. & Jung, H. T. Effect of SWNT defects on the electron transfer properties in P3HT/SWNT hybrid materials. *Adv. Funct. Mater.* **18,** 2659–2665 (2008).
38 Berson, S., de Bettignies, R., Bailly, S., Guillerez, S. & Jousselme, B. Elaboration of P3HT/CNT/PCBM composites for organic photovoltaic cells. *Adv. Funct. Mater.* **17,** 3363–3370 (2007).
39 Kim, K., Shin, J. W., Lee, Y. B., Cho, M. Y., Lee, S. H., Park, D. H., Jang, D. K., Lee, C. J. & Joo, J. Poly (3-hexylthiophene)/multiwalled carbon hybrid coaxial nanotubes: nanoscale rectification and photovoltaic characteristics. *ACS Nano* **4,** 4197–4205 (2010).
40 Wang, J. J., Cao, F. F., Jiang, L., Guo, Y. G., Hu, W. P. & Wan, L. J. High performance photodetectors of individual InSe single crystalline nanowire. *J. Am. Chem. Soc.* **131,** 15602–15603 (2009).

Supplementary Information accompanies the paper on the NPG Asia Materials website (http://www.nature.com/am)